Mechanisms Active during Fracture under Constraint

Robert F. Cook and Z. Suo

Abstract

Many advanced technologies center on devices of small feature sizes made of diverse materials. Internal stresses that arise in the devices during fabrication and use can result in fracture. Fracture of an individual feature in such a device may impair the function of the device. The materials surrounding the feature have a constraining effect on the elastic energy available to drive the fracture, the plastic flow associated with the fracture, and sometimes even the atomic processes at the crack tip. This article reviews fracture behavior in small structures, several distinct roles played by plasticity, and bond-breaking kinetics. Research challenges are also outlined.

Keywords: *adhesion, brittle materials, ductility, fracture, stress modeling, thin films.*

Introduction

Fracture at small length scales is a concern in many advanced technologies. Microelectronic, magnetic storage, and photonic devices make great use of oxide, nitride, and carbide dielectrics in submicrometer multilayer thin-film form. Liquid-crystal displays and optical fibers consist of glasses in sheet, particle, and fiber form. High-temperature turbines and engines rely on ceramic thermal-barrier coatings for blades and cylinders. Structural composites of all sorts use particles, whiskers, fibers, and platelets. These constrained geometries localize cracking so that fracture may not compromise the structural integrity of the entire component, but it may still impair the component's electrical, magnetic, optical, or thermal functions. For example, localized fracture of a dielectric film adjacent to a conducting line in a microelectronic chip-interconnection structure leads to electrical failure of the chip (which is of great importance), but not structural failure (which is of minor importance).

Thin-film fracture is a widely studied example of constrained fracture. Several cases are shown in Figures 1a–1d, including film splitting under tension, in which cracking occurs perpendicular to the film–substrate interface; film delamination under tension, in which cracking occurs parallel to the film–substrate interface, either at the interface (adhesive failure) or in the substrate (cohesive failure); and film delamination under compression, in which cracking occurs at the film–substrate interface and is accompanied by the formation of spherical or "telephone cord" buckled film caps. These examples highlight a feature common to fracture under constraint: The driving force usually derives not from a global stress applied by an external agency, but instead from an internal reaction stress to an imposed strain mismatch. Such strain mismatches arise from coefficient of thermal expansion (CTE) differences (giving rise to "thermal" stresses), phase transformations, mass transport (e.g., electromigration), and nonequilibrium processing conditions (giving rise to "athermal" stresses).[1]

The challenge in understanding constrained fracture is twofold: (1) to generate a continuum framework to encompass the diverse phenomena associated with the *geometrical* constraints on fracture, and (2) to incorporate atomistic concepts to describe the bond-breaking processes at the crack tip and the deformation processes away from the crack tip. This article describes the progress in addressing these challenges, drawing on several previous reviews[2–6] and the more recent literature. Study of fracture under constraint focuses more on continuum *mechanics* than atomic processes because constraint usually alters the energetics of fracture, but not the means by which bonds break. By contrast, in constrained plasticity, the existence and mobility of the strain-carrying agents (e.g., dislocations) are directly influenced by constraint.

Fracture Energies and Crack Driving Forces

The influence of constraint on fracture is illustrated in Figure 2. In Figure 2a, a crack of length c has been inserted into a freestanding sheet of thickness h, initially under a uniform applied stress σ_A. The sheet is large, and the stress is applied by loading grips far from the crack. The grips are held with no displacement and do no work during crack insertion. Two internal energy changes accompany the insertion of the crack: a surface energy increase associated with the surface area created, ΔU_S, and an elastic-strain energy reduction in a volume adjacent to the crack, ΔU_E. The change in total internal energy is

$$\Delta U = \Delta U_S + \Delta U_E. \quad (1)$$

The surface energy scales with the area of the crack, ch. The elastic energy scales with the volume of material in which the elastic energy is relaxed by the crack. In this case, the volume is approximately c^2h. These give ΔU as[7]

$$\Delta U = 2\gamma ch - \psi^2 \frac{\sigma_A^2}{E} c^2 h \quad \text{(freestanding sheet)}, \quad (2)$$

where γ is the surface-energy density, and the factor of 2 arises from the two crack faces. The term σ_A^2/E is a characteristic elastic-energy density (per volume), where E is Young's modulus. The dimensionless factor ψ takes into account the exact geometrical details of the volume of material affected by the crack and can be determined by solving the appropriate elasticity boundary-value problem. The free energy now takes on the character of a classic nucleation problem (Figure 3a). At small crack lengths, the surface energy dominates and the energy increases with crack length; the crack must heal to reduce the free energy. At large crack lengths, the elastic energy dominates and the energy decreases with crack length; the crack must grow to reduce the free energy. At an intermediate crack length, the free energy passes through a maximum corresponding to an unstable equilibrium state.

In Figure 2b, a crack of length c has been inserted into a thin film on a substrate. Prior to the insertion of the crack, the film is under a uniform tensile stress σ_F. The substrate constrains elastic deformation to

a length scale adjacent to the crack of approximately the film thickness. Consequently, the volume of material in which the elastic energy is relaxed now scales with ch^2. This gives[2]

$$\Delta U = 2\gamma ch - \psi^2 \frac{\sigma_F^2}{E} ch^2$$

(constrained film). (3)

The dimensionless factor ψ characterizes the film–substrate interaction: whether, for example, the film slides on the substrate, the substrate is rigid, the film is constrained on one or both faces, or there are adjacent film cracks. (Equation 3 strictly describes the long-crack, steady-state limit, $c >> h$, where ψ is independent of crack length c. For a short crack, $c \leq h$, the substrate constraint is not perceived, and there is a crack-length dependence of ψ such that Equation 2 pertains as $c \rightarrow 0$.) The change in energy with crack length is shown in Figure 3b. For film stresses large enough, the total change in energy appears superficially the same as that for the unconstrained body: at an intermediate critical crack length, the energy change passes through a maximum characterizing a point of unstable equilibrium and the competition between the surface and volume terms. There is, however, a qualitative difference between the allowed behaviors of the constrained and unconstrained bodies: the linear crack-length dependence of the elastic-energy change for the constrained film leads to the possibility that the film stress may be too low and no equilibrium condition can be met at any crack length. Such a variation in energy is shown as the dashed response in Figure 3b. The quadratic crack-length dependence of the elastic-energy change means that this is never true for the unconstrained body.

In Figure 2c, a crack of length c has been inserted into a body that is free but under the influence of a localized stress, arising, say, adjacent to a particle or fiber inclusion in a body or at an elastic or plastic contact on a body. Such stresses decay radially from a peak value of σ_P to zero over the characteristic length scale a of the inclusion. In the long-crack limit, $c >> a$, the stress field appears as a localized loading of characteristic force $P = \sigma_P a^2$. For a plane system, in which the stress decays quadratically from the peak value, the total change in energy is[8]

$$\Delta U = 2\gamma ch - \psi^2 \frac{\sigma_P^2}{E} \frac{a^4}{h} \ln(c/a)$$

(localized stress). (4)

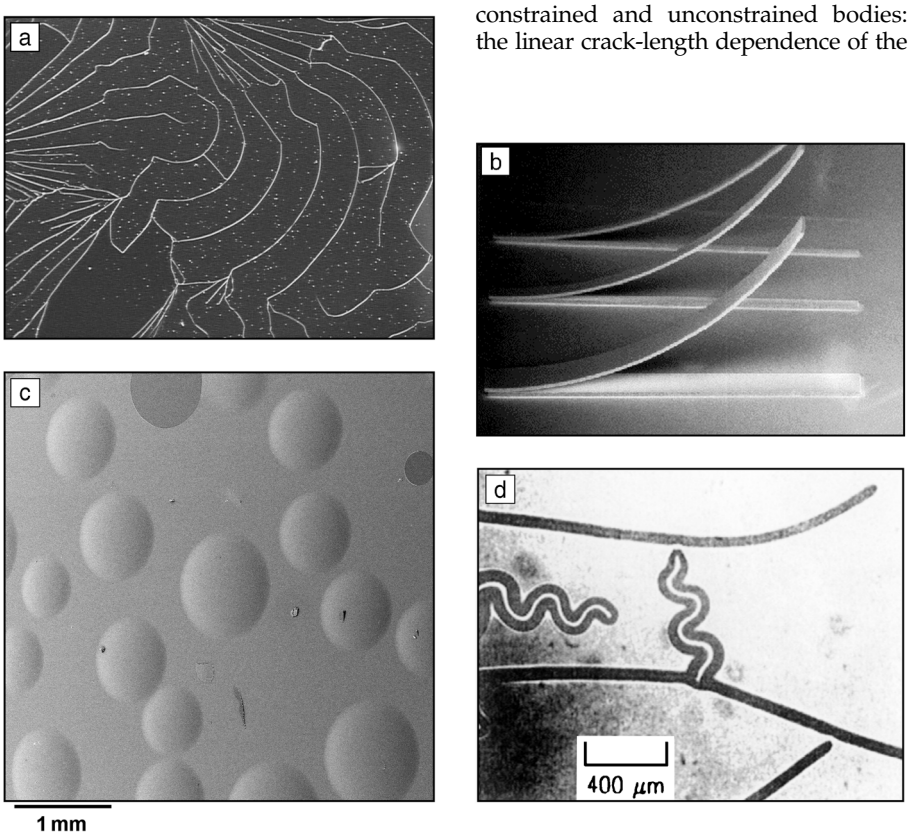

Figure 1. (a) Dark-field optical micrograph of a 4-μm-thick, 2.2-mm-wide film of amorphous hydrogenated Si deposited on a crystalline Si substrate. In-plane residual tensile stress arising from structural mismatch developed during film annealing leads to fracture of the film perpendicular to the film–substrate interface and film splitting or channel cracking. (Courtesy J. Thurn, University of Minnesota.) (b) Scanning electron microscopy (SEM) image of 400-μm-long film strips containing residual tensile stress arising from thermal-expansion mismatch with the substrate. The tensile stress leads to fracture parallel to the film–substrate interface and strip debonding. As a debond front approaches the remaining intact edge of a film strip, the debond driving force decreases, leading to debond arrest. (Courtesy Q. Ma, Intel Corp.) (c) SEM image of an amorphous hydrogenated Si film deposited on a crystalline Si substrate. In-plane compressive stress arising from structural mismatch developed during heating leads to debonding of the film–substrate interface and buckling of the film into spherical caps. (Courtesy J. Thurn, University of Minnesota.) (d) Optical micrograph of an amorphous Si film on a glass substrate. In-plane compressive stress in this case leads to debonded buckle tunnels extending underneath the film, either straight-sided or meandering (from Reference 3).

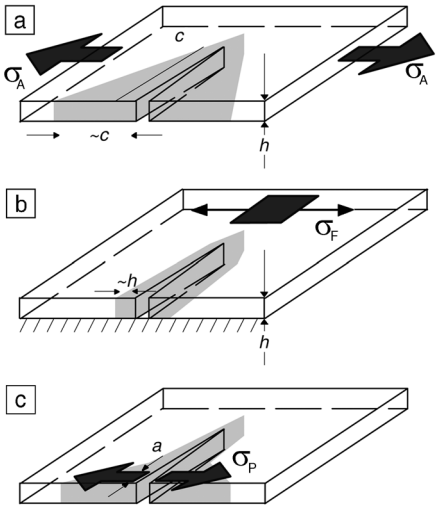

Figure 2. Schematic diagrams of bodies containing cracks under different levels of constrained loading: (a) freestanding sheet containing a through-crack under a uniform applied tensile stress, σ_A; (b) sheet attached to a substrate containing a channel crack under a film stress, σ_F; and (c) sheet containing a through-crack loaded locally by a stress σ_P over a region a. *In each case, the sheet thickness is* h *and the crack length is* c. *The volume of material in which the elastic-strain energy is affected by the crack is indicated as the shaded region.*

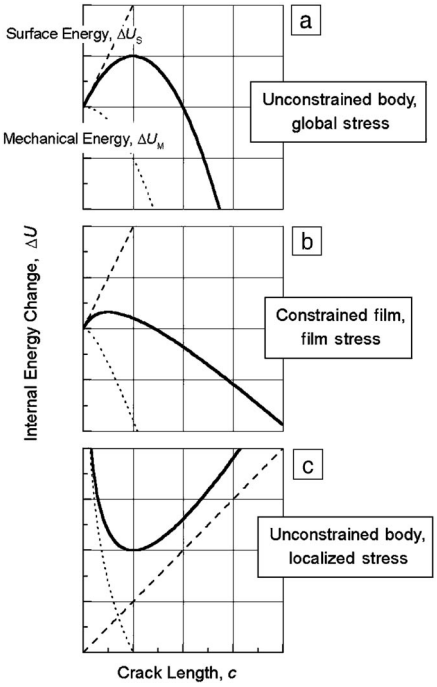

Figure 3. (a)–(c) Representative plots of the internal (mechanical and surface) energy changes accompanying crack insertion into bodies under various constraints (from Equations 2, 3, and 4). The total internal energy changes with crack length, shown by the solid lines, indicating the existence of unstable, neutral, or stable equilibria, depending on the degree of constraint of the fracture system.

(Once again, Equation 4 strictly describes the long-crack limit $c >> a$; in the short-crack limit, $c \leq a$, the stress decay is not perceived, and there is a crack-length dependence of ψ such that Equation 2 pertains as $c \rightarrow 0$.[9]) The total change in energy in the long-crack limit now takes on the character of a classic "bead-on-a-string" problem (Figure 3c). At small crack lengths, the volume term dominates, and the energy decreases with crack length. At large crack lengths, the surface term dominates, and the energy increases with crack length. The total energy minimizes at an intermediate crack length corresponding to a stable equilibrium state. Figure 4 shows an example of stable equilibrium cracks generated by localized loading associated with sharp contact.

The driving force for fracture G is a configurational force defined by the rate of release of elastic energy with crack area A:[7]

$$G = -\frac{\partial U_E}{\partial A}. \quad (5)$$

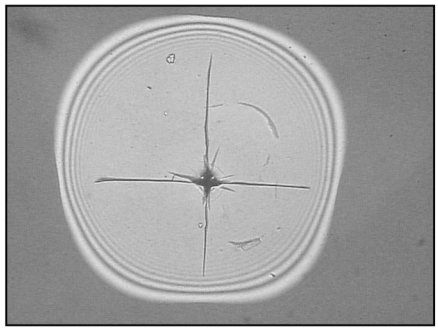

Figure 4. Optical micrograph of a Vickers indentation in a 17-μm amorphous AlO_x film deposited on an Al_2O_3-TiC substrate. The localized loading, evidenced by the central residual square indentation-contact impression, leads to stabilizing fracture fields for both radial (film-splitting) channel cracks and lateral (interface) debond cracks. (Courtesy J. Thurn, University of Minnesota.)

The partial derivative is taken by holding the displacement at the loading grips fixed. For the three examples here ($A = hc$), we have

$$G = \psi^2\sigma_A{}^2c/E \text{ (unconstrained body, global stress)}, \quad (6)$$

$$G = \psi^2\sigma_F{}^2h/E \text{ (constrained film, film stress, } c >> h), \quad (7)$$

and

$$G = \psi^2\sigma_P{}^2a^4/Eh^2c \text{ (unconstrained body, localized stress, } c >> a). \quad (8)$$

For the unconstrained body under global stress (Equation 6), no dimension appears except for the crack length, and the crack driving force is *destabilizing* ($dG/dc > 0$). For the unconstrained body under localized stress (Equation 8), both the characteristic dimension of the stress field and the body dimension appear along with the crack length, and the crack driving force is *stabilizing* ($dG/dc < 0$). In the intermediate case of the constrained film (Equation 7), no dimension appears except for the film thickness, and the crack driving force is *neutral* ($dG/dc = 0$). The constraint tends to reduce destabilizing crack fields to either neutral or stabilizing.

Analogous to the crack driving force, fracture resistance R is defined by

$$R = \frac{dU_S}{dA}, \quad (9)$$

such that for the simple systems here ($R = 2\gamma$), equilibrium is given by

$$G = 2\gamma. \quad (10)$$

As discussed in a later section, crack velocity increases with positive perturbation from equilibrium ($G > 2\gamma$). Consideration of Equations 7 and 8 shows that if stress levels are increased enough under constrained conditions such that equilibrium conditions are exceeded, cracks in films will propagate at constant velocity, and cracks adjacent to inclusions or contacts will propagate with decreasing velocity. That is, cracks in neutral driving fields propagate in a steady-state manner, cracks in stabilizing fields propagate in a decelerating, equilibrating manner.

Techniques suitable for measuring the fracture resistance of a material in small bodies have been reviewed.[4,10] For brittle materials, the fracture resistance is unaffected by the smallness of the body. However, as many materials used in advanced technologies have far-from-equilibrium microstructures, with no bulk analogues, measurements at small scales are often necessary.

Fracture in Thin-Film Structures

Channel and Tunnel Cracking

Perhaps the simplest fracture constraint is to limit deformation adjacent to the crack tip through the presence of a stiff substrate, or substrate-plus-"cap" combination. This effect is quantified through the dimensionless factor ψ by solving elastic boundary-value problems.[2] For example, for the film crack shown in Figure 2b, $\psi = 1.4$ when the film and substrate are of equal moduli. The driving force for such "channel" cracks is reduced if the substrate has a greater modulus than the film; $\psi = 1.1$ for a compliant film on a rigid substrate. "Capping" a film with a layer that remains intact during crack propagation in the film leads to "tunnel" cracks. The limit for a compliant film sandwiched between a rigid substrate and a rigid cap is $\psi = 0.71$. The quadratic dependence of the crack driving force G on ψ, and a usually exponential dependence of crack velocity v on G, leads to tremendous suppression of channel- or tunnel-crack extension through the use of constraining, stiff underlayers or overlayer caps. Of course, suppression of such film-splitting cracks only appears if the film and substrate or cap remain bonded.

Delamination Fracture

A film under a tensile stress may debond at the film–substrate interface from the root of a channel crack or from a free edge

(Figure 1b). When the debond length c is short compared with film thickness h, the driving force is sensitive to the detailed geometry. When $c \geq h$, the delamination process attains a steady state, and the driving force becomes independent of the debond length. Under the plane-strain conditions, this neutral debond driving force is given by Equation 7 with $\psi = 0.71(1 - \nu_F^2)$, where ν_F is the Poisson ratio of the film. Delamination releases the full elastic-strain energy density of the film, $\sigma_F^2/2E^*$, where $E^* = E_F/(1 - \nu_F^2)$ is the plane-strain modulus of the film. The fracture resistance of the interface ($R = \Gamma_i$) is usually different from either the film or substrate, such that equilibrium is given by $G = \Gamma_i$.

The debond crack is under mixed-mode loading: on the interface ahead of the crack there is both mode I tensile stress and mode II shear stress. For example, when the film and the substrate have identical elastic constants, the modes I and II stress-intensity factors, K_I and K_{II}, are given by

$$K_I = \sigma_F \sqrt{\frac{h}{2}} \cos \omega, K_{II} = \sigma_F \sqrt{\frac{h}{2}} \sin \omega, \tag{11}$$

with $\omega \approx 52°$. Modulus mismatch between the film and the substrate alters the degree of mode mixing through the phase angle ω.[2] The debond resistance Γ_i depends on the degree of mode mixing. Methods to measure Γ_i as a function of the degree of mode mixing are discussed in References 2, 4, 11, and 12 and have been applied to microelectronic device structures[13] and thermal-barrier coatings.[14]

Buckle-Driven Fracture

When a film is under compression $\sigma_F < 0$, it may still exhibit constrained fracture as a debond from the substrate, but it will do so in quite different ways from a film under tension. To appreciate the basic behavior, first assume the plane-strain conditions as illustrated in Figure 5a. For a debond crack initiated from the edge of a film under compression, the debonded film remains in contact with the substrate. This can be understood as follows. If the two crack faces were not in contact, they would be traction-free, and the stress-intensity factors would be given by Equation 11. The residual stress in the film is now compressive so that $K_I < 0$, suggesting that although the two crack faces should be in contact, they may slide relative to each other. Such a crack will stop after a certain extension, that is, the constrained geometry in this case gives rise to a stabilizing field. Assuming that the sliding friction has a constant value τ_0, the stable equilibrium crack length l may be estimated by a shear-lag model in which force balance of the sliding segment of the film requires that $l\tau_0 = \sigma_F h$.

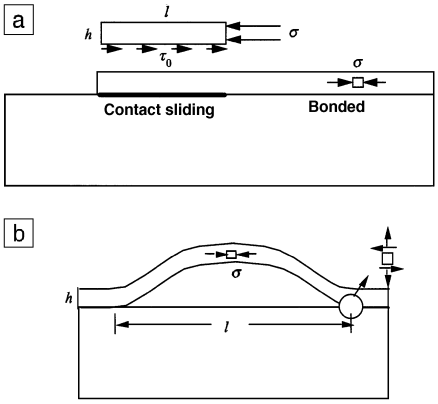

Figure 5. Schematic diagrams of the effects of compressive stress in a film initially bonded to a substrate. (a) A body containing a debond crack initiated from the edge of a film. (b) An unbonded film in the center of a body undergoing buckling. In the case of the center-crack + buckle, a crack-opening stress arises at the film–substrate interface.

Next consider the debond underneath a film, remote from the film edges. When the film is perfectly bonded with the substrate, the film is under compression, but the interface is stress-free. Even when an area underneath the film is unbonded, as long as the film remains flat, there is no stress acting on the interface. However, a large enough area of unbonded film may buckle (Figure 5b). After buckling, on the interface at the buckle front, both normal and shear stresses develop, which may motivate the unbonded area to grow like a crack. Three aspects need be considered: pre-buckling development of an unbonded area, buckling of the unbonded film, and post-buckling growth of the unbonded area.

Despite their practical significance, pre-buckling processes are difficult to quantify: a contaminated substrate may lead to large unbonded areas after a film is grown; non-planar interfaces can promote buckling;[15] interface voids are sometimes observed, leading to buckling; and a compressed elastic film can buckle while still bonded to the substrate, if the substrate has very low elastic stiffness[16] or creeps.[17] A thermally grown oxide on a plastically deformable substrate can buckle, provided that cyclic temperature changes and continued oxidation inside the film repeatedly bring the substrate into the yield condition.[18] Various processes leading to fracture in thermal-barrier coatings have been described in which compressive stress in films is the main driving force.[19]

By contrast, film buckling is well understood. If the film has a sufficiently large unbonded area, the film over the area buckles. The critical unbonded length for buckling, l_c, is given by

$$\frac{l_c}{h} = \pi \left(\frac{E^*}{-3\sigma_F} \right)^{1/2}. \tag{12}$$

(This expression comes from Euler's solution for a buckling column, adjusted for the plane-strain conditions; save for the numerical pre-factor $\pi/3^{1/2}$, the form of the equation applies to an unbonded area of any shape, with the ratio of critical debond length to film thickness being inversely proportional to the square root of the film strain.) Taking $\sigma_F/E^* \sim 10^{-2}$, which is a rather large elastic strain, Equation 12 gives $l_c \sim 20h$. Such a large unbonded area is not usually produced in film growth. Consequently, to avert buckling failure, it pays to investigate the pre-buckling processes that produce large unbonded areas.

Several post-buckling behaviors have been studied.[2,20] Unlike a debond crack initiated from a film edge, a debond crack initiated from a buckled film does have an opening component at the crack front ($K_I > 0$). However, when the crack enlarges, the opening component reduces, the crack approaches the pure sliding mode, and the situation becomes indistinguishable from a debond crack initiated from the film edge. Consequently, a debond buckle under the plane-strain conditions will arrest by friction. Similarly, a circular (or any equiaxed) debond buckle cannot grow indefinitely. A debond buckle, however, can grow like a tunnel underneath the film, uninhibited laterally until it approaches another tunnel or an edge of the film (Figure 1c). If initiated from isolated, unbonded areas, such tunnels can cause an entire film to disintegrate.

Effects of Inelastic Deformation

In the foregoing, we have applied linear elastic-fracture mechanics (LEFM) to film–substrate composites. A main requirement of such applications is that the inelastic bond-rupture or plastic-deformation zone around the crack tip must be much smaller than the film thickness such that the inelastic deformation within this (small) zone is accounted for by the fracture resistance. In computing the crack driving force, both the film and the substrate are

taken to be elastic. When the inelastic zone is large compared with the film thickness, however, we must consider the inelastic deformation more explicitly. The following examples illustrate several distinct roles played by plasticity.

Loss of Constraint Due to Plastic Deformation

First consider a brittle film on a thick, ductile substrate. The film is under tension and is prone to channel cracking (Figure 2b). Because the film is elastic, the crack driving force at the channel front is well defined; to calculate this driving force, plastic deformation in the substrate must be accounted for in the resulting boundary-value problem. However, it is clear that if the substrate were elastic, it would constrain the opening displacement of the channel, so that the driving force at the channel front would be small. This constraint is reduced when the substrate deforms plastically. Consequently, plastic deformation in a substrate promotes channel cracking in a film.[21,22] The constraint is completely lost over time if the substrate creeps.

Cleavage Fracture in the Presence of Plastic Flow

As a second example, consider a two-layer film on a ductile substrate (Figure 6). The two materials constituting the film are both elastic, and a crack runs on the interface between them. Because the crack runs on the interface between two elastic materials, one can prescribe the debond resistance for this interface and account for plasticity in the substrate in the boundary-value problem in calculating the crack driving force.[23,24] The plastic hysteresis in the substrate costs energy and makes the debond crack more difficult to grow.

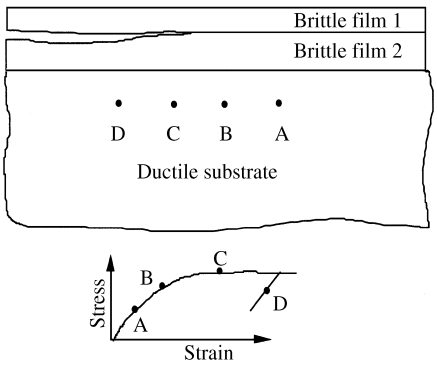

Figure 6. Schematic diagram of a debond crack propagating in elastic layers adjacent to a ductile substrate. As the debond tip passes, a material particle in the substrate undergoes a history of dissipative hysteretic deformation: elastic (A), yielding (B), plastic straining (C), and elastic unloading (D).

From a Structureless Crack Tip to the Cohesive-Zone Model

A third example involves a crack on the interface between a film and a substrate, and yielding can take place either in the film or in the substrate. In the previous discussions, the crack tip is taken to be a structureless mathematical point and the crack resistance a material constant. When one or both materials deform plastically, the crack tip on the interface blunts, the crack driving force cannot be defined at the crack tip, and there is no unambiguous way to partition plasticity between the fracture resistance and the crack driving force. To circumvent this difficulty, we must describe the fracture process with more details than a structureless crack tip encountering a constant fracture resistance. At one extreme, we can include all the individual atoms. Such a detailed model, however, may never replace the one-parameter fracture mechanics in practice. Less detailed descriptions are being considered. An economic description is the cohesive-zone model, which describes the fracture process by a relation of the separation and the traction between the two crack faces. When the cohesive zone is embedded in materials described by continuum plasticity, the model provides a framework to correlate experimental results.[5] Inelastic deformation can also be described by collective dislocation activity.[25]

Fracture Caused by Constrained Plastic Flow

As a fourth example, consider a thin metal film sandwiched between two elastic substrates.[26–28] A debond crack preexists on one of the interfaces, and the substrates are loaded to open the crack. Let h be the film thickness and r_p the plastic zone size on crack propagation. When $h >> r_p$, the substrates place no additional constraint on fracture. As the load increases and the crack tip blunts, the level of the peak stress remains constant (a few times the yield strength), and the location of the peak stress is about two times the crack-opening displacement ahead of the crack tip. The behavior is similar to ductile fracture of a bulk metal. When $h < r_p$, however, the substrates significantly constrain the plastic flow in the film. As the load increases and the crack tip blunts, the level of the peak stress in the metal increases, and the location of the peak stress is several times the film thickness ahead of the crack tip. The high stress activates flaws ahead of the crack tip into new debond areas, which link back to the main crack. When the film thickness is very small, the dislocations emitted from the crack tip pile up at the substrate–film interfaces. As the load increases and the crack tip blunts, more dislocations pile up, and the stress at the crack tip can increase up to the theoretical strength. Even fcc metals can fracture by cleavage this way. This is perhaps an ultimate form of constraint.

Fatigue: Ratcheting-Induced Fracture

The last example concerns a recently discovered fracture mechanism. Temperature cycling is a method often used to test or qualify the reliability of microelectronic devices. Because of CTE mismatch among various materials in such devices, the cyclic temperature causes repeated changes in stress and strain throughout the structure. Fatigue failure of ductile materials in the device, such as solder joints and polymer underfills, has been commonly observed. In some device structures, it has also been observed that cyclic temperature causes progressive cracking in brittle materials.[29–31] This intriguing behavior has been understood as follows. The cyclic temperature can cause plastic deformation in a ductile material adjacent to the brittle material. Under certain conditions, the plastic deformation accumulates in one direction as the temperature cycles. Such deformation is known as ratcheting deformation. As the ductile material ratchets, the accumulated deformation causes a large stress in the brittle material, leading to cracking.

Kinetic Effects in Constrained Fracture

These considerations, focusing on the equilibrium behavior of constrained fracture systems, show that inclusion of the new length scale characterizing the constraint, usually a film thickness, changes crack behavior from that occurring in a free body. Nonequilibrium fracture processes bring their own length and energy scales, typically characterizing the (noncontinuum) details of the kinetics of the bond-rupture process. For example, thermally activated bond rupture is described by an (average) bond separation a, an energy required for bond rupture u_0, and an activation energy for bond rupture u_1, such that the observed crack velocity v is given by[32,33]

$$v = v_0 \sinh[(G - 2\gamma/\eta]/B, \qquad (13)$$

where the macroscopic crack-velocity parameters are related to the bond-scale parameters and temperature T by

$$\eta = 2kT/a^2,$$

$$2\gamma = u_0/a^2,$$

and

$$v_0 = 2af_0 \exp(-u_1/kT), \tag{14}$$

where f_0 is a characteristic attempt frequency for bond rupture (and healing), and k is the Boltzmann constant. The connection between the crack velocity and the constrained behavior of the fracture system comes in through the general $G - 2\gamma$ term in Equation 13, which characterizes the degree of departure of the system from equilibrium and how that varies with crack length (noting that the condition $G = 2\gamma$ does indeed give $v = 0$), and more specifically through the B term, which characterizes the number of bond sites on the crack periphery:

$$B = dA/adc, \tag{15}$$

where A is the crack area. For channel, tunnel, or plane-strain buckle cracks constrained in a film, $dA/dc = h$ is a constant, such that for fracture systems a long way from equilibrium ($G >> 2\gamma$), the crack velocity is both enhanced (greater driving force from $G \propto h$) and impeded (slower kinetics from $v \propto 1/h$) by increasing film thickness:

$$v \propto \frac{\exp(h/\eta)}{h}. \tag{16}$$

Under usual circumstances, the degree of thermal activation given by η is such that the exponential term dominates, and crack velocity increases dramatically for cracks in thicker films. An example is shown in Figure 7 for channeling cracks in a tensile dielectric film. Similar considerations apply to interfacial debonding cracks.[24] For buckle cracks constrained to be circular or elliptical, $dA/dc = 2\pi c$ is not constant, and such fracture systems are doubly impeded in crack velocity (decreased perturbation from equilibrium, $G - 2\gamma \propto 1/c$, and slower kinetics, $v \propto 1/c$),

$$v \propto \frac{\exp(1/c)}{c}, \tag{17}$$

and such cracks arrest very quickly on crack extension, as might be inferred from the spherical buckle caps in Figure 1.

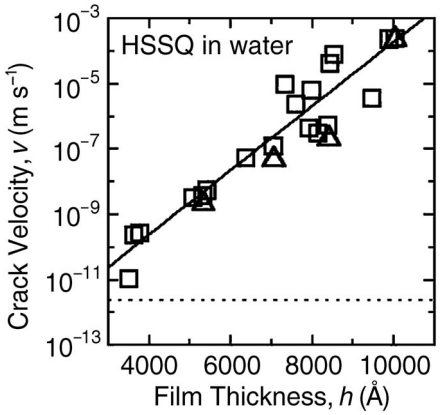

Figure 7. Plot of velocity of channel cracks versus film thickness for a low-dielectric-constant hydrogen silsesquioxane (HSSQ) tensile film in water.[33] The exponential dependence is symptomatic of stress-corrosion cracking in a system far from equilibrium. Open squares (□) represent measurements made using films with deliberately induced indentation flaws; open triangles (△) represent measurements made using samples with naturally occurring intrinsic flaws. The dotted line is an exponential best fit, as suggested by Equation 16.

Challenges

The mechanics of fracture under constrained conditions has been extensively investigated over the last decade, especially when the constituents are elastic. There are many applications of such mechanics to the technologically important geometry of thin films or coatings on substrates, although fracture adjacent to fibers and other inclusions is also much studied. The extension of such analyses to include plasticity is usually made through adjustment of boundary conditions when fracture is still restricted to an elastic medium, or through adjustment of fracture-resistance for small-scale yielding in a plastic medium. Many analytical challenges remain, however. These include the explicit incorporation of cycle- or time-dependence for plastic or viscous deformation; the extension of fracture mechanics to more exotic geometries, such as arise in microelectromechanical systems (MEMS) structures; the inclusion of atomic-scale considerations of fracture mechanisms for cracks restricted to very small elements, such that the cohesive zone is comparable to the crack size; coupling of fracture to piezoelectric and piezomagnetic effects, such as occur in capacitors, actuators, and magnetic-storage devices; nonequilibrium fracture that is not reaction-limited but transport-limited, especially at interfaces; greater consideration of the stability of fracture paths, not just criteria for crack extension, such that geometry and forces are important, not just fracture energetics; and extensions to nonlinear mechanics for relatively large-deformation, high-strength structures. Experimental challenges also abound: experimental methods for examining fracture at small scales or in constrained geometries are few. Those that offer promise are *in situ* and environmental scanning electron microscopy observation of fracture specimens and components and scanning probe microscopy methods, especially those associated with depth-sensing indentation. Finally, a small structure may take more time to nucleate a crack than to grow a crack. Crack nucleation usually results from microstructural changes, for example, phase coarsening,[34] dislocation activity,[35] or mass erosion.[36] Theoretical and experimental studies of the crack-nucleation process remain a great challenge.

Acknowledgments

The work of R.F. Cook has been supported by Seagate Technology and International Sematech. The work of Z. Suo has been supported by the Intel Corp., the New Jersey Science and Technology Commission, and the Multi-University Research Initiative (MURI).

References

1. W.D. Nix, *Metall. Trans. A* **20A** (1989) p. 2217.
2. J.W. Hutchinson and Z. Suo, *Adv. Appl. Mech.* **29** (1992) p. 63.
3. M.D. Thouless, *J. Vac. Sci. Technol., A* **A9** (1991) p. 2510; *J. Am. Ceram. Soc.* **76** (1993) p. 2936.
4. A.G. Evans and J.W. Hutchinson, *Acta Metall. Mater.* **43** (1995) p. 2507.
5. J.W. Hutchinson and A.G. Evans, *Acta Mater.* **48** (2000) p. 125.
6. Z. Suo, in *Encyclopedia of Materials: Science and Technology,* 2nd ed. (Elsevier Science, New York, 2001) in press.
7. B.R. Lawn, *Fracture of Brittle Solids,* 2nd ed. (Cambridge University Press, Cambridge, 1993).
8. R.F. Cook and G.M. Pharr, in *Materials Science and Technology,* edited by R.W. Cahn, P. Haasen, and E.J. Kramer (VCH, Weinheim, 1994) p. 339.
9. T.C. Lu, J. Yang, Z. Suo, A.G. Evans, R. Hecht, and R. Mehrabian, *Acta Metall. Mater.* **39** (1991) p. 1883.
10. Q. Ma, J. Xia, S. Chao, S. El-Mansy, R. McFadden, and H. Fujimoto, in *Materials Reliability in Microelectronics VIII,* edited by J.C. Bravman, T.N. Marieb, J.R. Lloyd, and M.A. Korhonen (Mater. Res. Soc. Symp. Proc. **516**, Warrendale, PA, 1998) p. 331.
11. M.D. Drory and J.W. Hutchinson, *Proc. R. Soc. London, Ser. A* **452** (1996) p. 2319.
12. K.M. Liechti and Y.S. Chai, *J. Appl. Mech.* **58** (3) (1991) p. 680.
13. R. Dauskardt, M. Lane, Q. Ma, and N. Krishna, *Eng. Fracture Mech.* **61** (1) (1998) p. 141.
14. J.L. Beuth (unpublished manuscript).

15. J.W. Hutchinson, M.Y. He, and A.G. Evans, *J. Mech. Phys. Solids* **48** (2000) p. 709.
16. W.T.S. Huck, N. Bowden, P. Onck, T. Pardoen, J.W. Hutchinson, and G.M. Whitesides, *Langmuir* **16** (2000) p. 3497.
17. N. Sridhar, D.J. Srolovitz, and Z. Suo, *Appl. Phys. Lett.* **78** (2001) p. 2482.
18. M.Y. He, A.G. Evans, and J.W. Hutchinson, *Acta Mater.* **48** (2000) p. 2593.
19. V.K. Tolpygo and D.R. Clarke, in *Elevated Temperature Coatings: Science and Technology IV,* edited by N.B. Dahotre, J.M. Hampikian, and J.E. Morral (The Minerals, Metals & Materials Society, Warrendale, PA, 2001) p. 93.
20. G. Gioia and M. Ortiz, *Adv. Appl. Mech.* **33** (1997) p. 119.
21. M.S. Hu and A.G. Evans, *Acta Mater.* **37** (1989) p. 917.
22. J.L. Beuth and N.W. Klingbeil, *J. Mech. Phys. Solids* **44** (1996) p. 1411.
23. Z. Suo, C.F. Shih, and A.G. Varias, *Acta Metall. Mater.* **41** (1993) p. 1551.
24. M. Lane, R.H. Dauskardt, A. Vainchtein, and H.J. Gao, *J. Mater. Res.* **15** (12) (2000) p. 2758.
25. A. Needleman and E. van der Giessen, *MRS Bull.* **26** (3) (2001) p. 211.
26. A.G. Varias, Z. Suo, and C.F. Shih, *J. Mech. Phys. Solids* **39** (1991) p. 963.
27. K.J. Hsia, Z. Suo, and W. Yang, *J. Mech. Phys. Solids* **42** (1994) p. 877.
28. S.X. Mao and A.G. Evans, *Acta Mater.* **45** (10) (1997) p. 4263.
29. M. Huang, Z. Suo, Q. Ma, and H. Fujimoto, *J. Mater. Res.* **15** (2000) p. 1239.
30. M.R. Begley and A.G. Evans, *Trans. ASME J. Appl. Mech.* in press.
31. M. Huang, Z. Suo, and Q. Ma, *J. Mech. Phys. Solids* in press.
32. R.F. Cook and E.G. Liniger, *J. Am. Ceram. Soc.* **76** (1993) p. 1096.
33. R.F. Cook and E.G. Liniger, *J. Electrochem. Soc.* **146** (1999) p. 4439.
34. Y. Wei, C.L. Chow, H.E. Fang, M.K. Neilsen, T.J. Lim, and W. Lu (unpublished manuscript).
35. S. Suresh, *Fatigue of Materials* (Cambridge University Press, Cambridge, 1998).
36. H.H. Yu and Z. Suo, *Acta Mater.* **47** (1999) p. 77. □